All about Athena

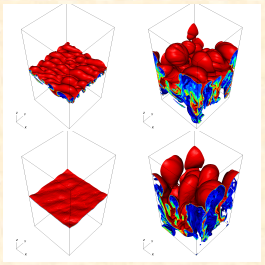

(Five lectures)

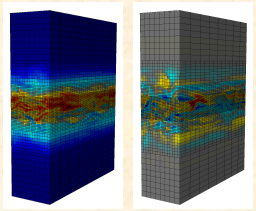

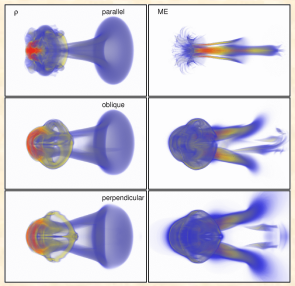

Jim Stone
Department of Astrophysical Sciences
Princeton University

Outline of lectures

Lecture 1. Introduction to basic algorithm

Lecture 2. Grids in grid codes

Lecture 3. Extra physics

Lecture 4. Radiation hydrodynamics

Lecture 5. Example applications; future developments

Outline of Lecture 2:

1. Alternatives to structured grids
2. Galilean invariance of grid codes.
3. Cylindrical (curvilinear) grids
   - Algorithm
   - Tests
4. Static mesh refinement (SMR) in Athena
   - Prolongation
   - Restriction
   - Flux correction
   - Implementation

Athena uses a regular, structured mesh.

Cell-centered mass, momentum, energy; face-centered field:

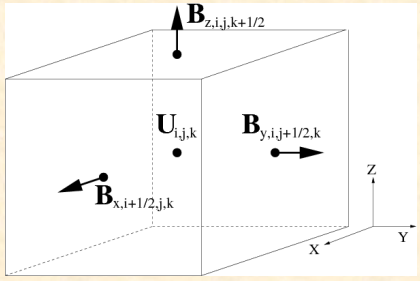

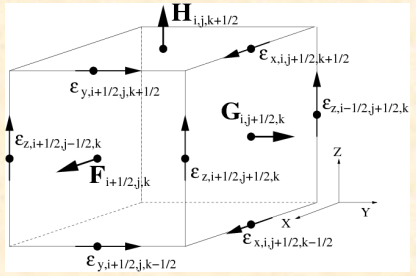

Face-centered fluxes, and edge-centered EMFs.

Alternatives to structured Eulerian mesh.

- Spectral methods
- Unstructured Eulerian mesh
- Lagrangian mesh
- Particle methods (SPH)
- Arbitrary Langrangian-Eulerian (ALE) methods using either structured or unstructured meshes (moving mesh methods)

Each method has its pros and cons. Each is best for certain kinds of problems. No one is best for all problems.

Galilean invariance of grid codes

Recently, Springel (2009) has reported grid codes produce different results when the calculations are run in different frames of reference (by adding constant background velocity).

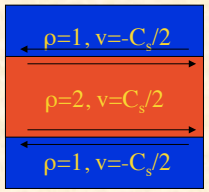

e.g. Kelvin-Helmholtz instability between different density shear layers

Add long wavelength perturbation $V_y=A\sin(4\pi x/L_x)$

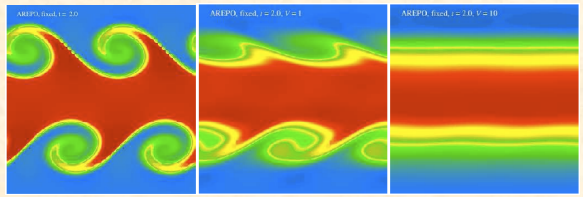

$V_0/C_s = 0$ $V_0/C_s = 1$ $V_0/C_s = 10$

Galilean invariance of grid codes

This has widely been interpreted as "Fixed grid codes produce solutions which are not Galilean invariant".

If true, this would mean grid codes are useless, because the solutions they produce are completely incorrect.

If true, this would violate the Lax-Wendroff theorem, which states conservative, consistent, convergent numerical schemes are guaranteed to converge to the correct solution.

The reported lack of Galilean invariance of grid codes is based on a misunderstanding of the roles of truncation error and convergence in numerical solutions.

Do not make this mistake yourself!

Convergence demonstrates solutions computed with Athena are Galilean invariant

The Gresho vortex test in two dimensions

CONVERGENCE RATE AGAINST ANALYTIC SOLUTION FOR AREPO AND ATHENA

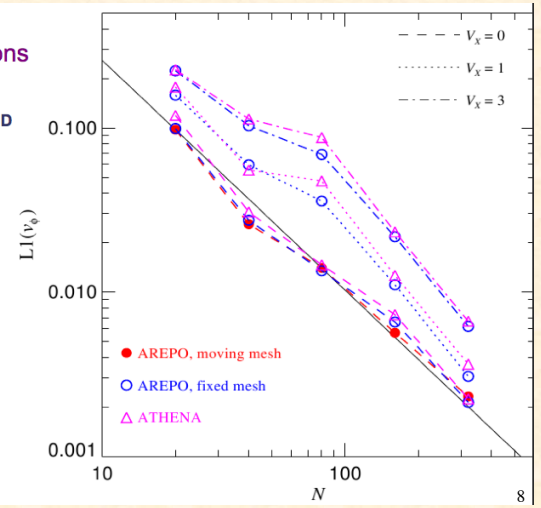

Should we be worried about change in truncation error with velocity?

Perhaps. If dominant source of error in your application is due to advection, then reducing this error will help.

But. In most codes reducing error in velocity is at the expense of increasing error in other ways, e.g. using an unstructured mesh to represent multidimensional flows.

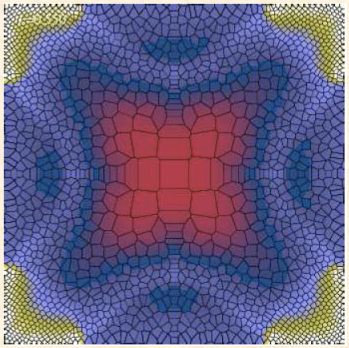

Blast test from Springel (2009)

The fact that the truncation error is different in different frames does not mean the solution violates Galilean invariance (just that the truncation error does).

Fact that truncation error changes solution well known from convergence tests, e.g. repeat KH test with V_0=0 and different numerical resolutions. Which is the correct solution that should be reproduced in all frames?

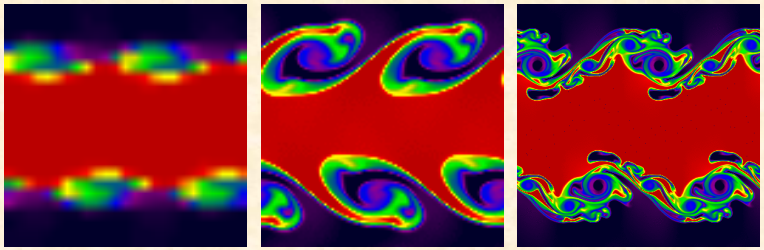

25^2 100^2 400^2

KH test for *resolved* solutions.

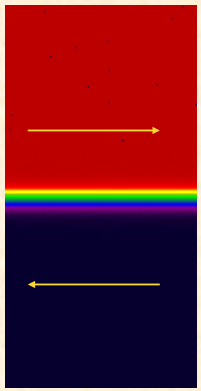

Study KH instability across a resolved shear layer in constant density fluid.

$V_x = (C_s/2)\tanh(y/a)$
Add long wavelength perturbation $V_y=\sin(4\pi x/L_x)$

Boost solution to different frames using constant $V_0 = 100\ C_s$. *This is a tough test!*

Solution for a resolved KH mode

Images of $\delta V_x = V_x - V_0$ and V_y at t=4.64 (peak of growth)

Which one is moving, which one is at rest???

δV_x

V_y

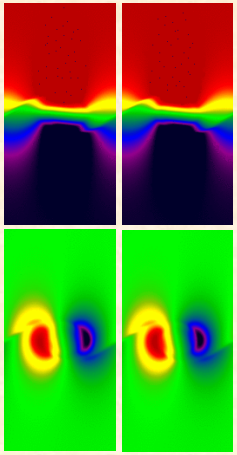

Color scale:
+/- $C_s/2$ in all images

Solution for a resolved KH mode

Images of $\delta V_x = V_x - V_0$ and V_y at t=4.64 (peak of growth)

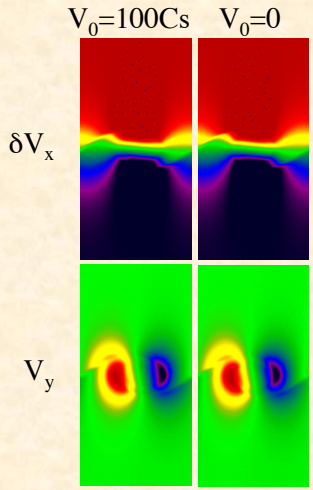

Color scale:
+/- $C_s/2$ in all images

Solutions are quantitatively identical.

Time evolution of KE in transverse component of velocity.

Linear growth rate of instability captured correctly in both cases.

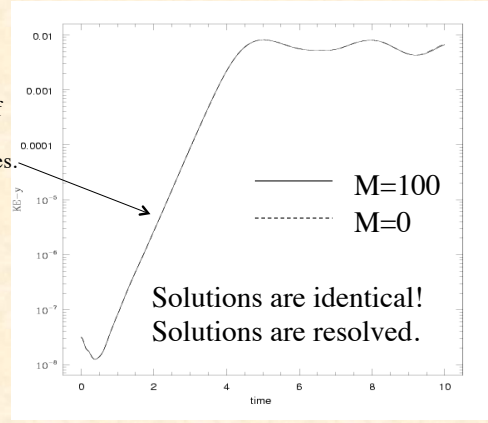

Dynamics of resolved KH instability has been correctly captured in both frames remarkably well.

Fixed grid codes converge to solutions which are Galilean invariant.

Period.

Following slides on cylindrical grid courtesy A. Skinner:

Motivation for curvilinear coordinates

Many astrophysical systems of interest, including disk systems, winds, and jets, exhibit some sort of cylindrical geometry. Furthermore, angular momentum preservation is superior for rotating, grid-aligned flows, and imposition of boundary conditions is much simpler compared to the Cartesian-grid case.

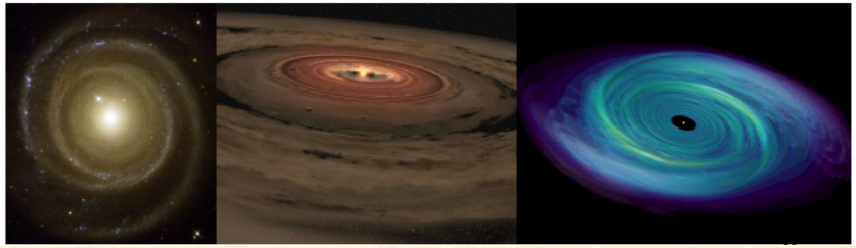

Equations in cylindrical coordinates

Momentum equation in cylindrical coordinates

$$\frac{\partial}{\partial t}(\rho v_R) + \frac{1}{R}\frac{\partial}{\partial R}(R\,M_{RR}) + \frac{1}{R}\frac{\partial}{\partial \phi}M_{\phi R} + \frac{\partial}{\partial z}M_{zR} = \frac{M_{\phi\phi}}{R} \quad (1)$$

$$\frac{\partial}{\partial t}(\rho v_\phi) + \frac{1}{R^2}\frac{\partial}{\partial R}\left[R^2 M_{R\phi}\right] + \frac{1}{R}\frac{\partial}{\partial \phi}(M_{\phi\phi}) + \frac{\partial}{\partial z}(M_{z\phi}) = 0, \quad (2)$$

$$\frac{\partial}{\partial t}(\rho v_z) + \frac{1}{R}\frac{\partial}{\partial R}(R\,M_{Rz}) + \frac{1}{R}\frac{\partial}{\partial \phi}M_{\phi z} + \frac{\partial}{\partial z}M_{zz} = 0, \quad (3)$$

where $M_{ij} \equiv \rho v_i v_j - B_i B_j + P^* \delta_{ij}$. $M_{\phi\phi}/R$ includes centrifugal force and magnetic tension terms.

Equation (2) is actually in angular momentum preserving form, which has no source term.
The implemented Riemann solvers only compute linear momenta.

Induction equation in cylindrical coordinates

$$\frac{\partial}{\partial t}B_R + \frac{1}{R}\frac{\partial}{\partial \phi}J_{\phi R} + \frac{\partial}{\partial z}J_{zR} = 0, \quad (4)$$

$$\frac{\partial}{\partial t}B_\phi + \frac{\partial}{\partial R}J_{R\phi} + \frac{\partial}{\partial z}J_{z\phi} = 0, \quad (5)$$

$$\frac{\partial}{\partial t}(RB_z) + \frac{\partial}{\partial R}(R\,J_{Rz}) + \frac{1}{R}\frac{\partial}{\partial \phi}(RJ_{\phi z}) = 0, \quad (6)$$

where $J_{ij} \equiv v_i B_j - B_i v_j$.

Since we perform a finite *area* update on the magnetic field, the scale factors only appear in the B_z equation.

Reconstruction for CTU integrator

Computing the L/R states at time $t^{n+1/2}$

1. Reconstruct and limit in the characteristic variables
2. Evolve the constant-coefficient linear system exactly
3. Average the solution over the domain of dependence for each wave family

This method requires a complete set of eigenvalues (characteristic wavespeeds) and eigenvectors for the wave matrix $\mathbf{A}$.

Must also take care to distinguish geometric center of cell from volume center!

Projected linearized system - Cartesian coordinates

$$\partial_t \mathbf{w} + \mathbf{A}\,\partial_x \mathbf{w} = \mathbf{s}_{\rm MHD}, \quad (7)$$

where

$$\mathbf{A} = \begin{bmatrix} v_x & \rho & 0 & 0 & 0 & 0 & 0 \\ 0 & v_x & 0 & 0 & 1/\rho & B_y/\rho & B_z/\rho \\ 0 & 0 & v_x & 0 & 0 & -B_x/\rho & 0 \\ 0 & 0 & 0 & v_x & 0 & 0 & -B_x/\rho \\ 0 & \gamma P & 0 & 0 & v_x & 0 & 0 \\ 0 & B_y & -B_x & 0 & 0 & v_x & 0 \\ 0 & B_z & 0 & -B_x & 0 & 0 & v_x \end{bmatrix} \quad (8)$$

is the wave matrix linearized about the state $\mathbf{w}^n$, and $\mathbf{s}_{\rm MHD}$ is the MHD source (Gardiner & Stone 2005, 2008).

Projected linearized system - cylindrical coordinates

$$\partial_t \mathbf{w} + \mathbf{A}\,\partial_R \mathbf{w} = \mathbf{s}_{\rm MHD} + \mathbf{s}_{\rm geom}, \tag{9}$$

where $\mathbf{A}$ and $\mathbf{s}_{\rm MHD}$ are analogous to the Cartesian case, and

$$\mathbf{s}_{\rm geom} \equiv \begin{bmatrix} -\frac{1}{R}\rho v_R \\ \frac{1}{R}(v_\phi^2 - \frac{1}{\rho}B_\phi^2) \\ -\frac{1}{R}(v_\phi v_R - \frac{1}{\rho}B_\phi B_R) \\ 0 \\ -\frac{1}{R}\gamma P v_R \\ -\frac{1}{R}v_\phi B_R \\ -\frac{1}{R}v_R B_z \end{bmatrix} \tag{10}$$

is the geometric source term.

Source terms not needed for VL integrator.

Once fluxes have been computed (from the L/R states via the Riemann solver), the finite volume method (FVM) is used to update the volume-averaged quantities.

FVM Update in Cylindrical Coordinates

$$\begin{aligned}\mathbf{Q}_{ijk}^{n+1} = \mathbf{Q}_{ijk}^{n} &- \frac{\Delta t}{R_i\,\Delta R}\left(R_{i+1/2}\,\mathbf{F}^{n+1/2}_{R;\,i+1/2,j,k} - R_{i-1/2}\,\mathbf{F}^{n+1/2}_{R;\,i-1/2,j,k}\right) \\ &- \frac{\Delta t}{R_i\,\Delta\phi}\left(\mathbf{F}^{n+1/2}_{\phi;\,i,j+1/2,k} - \mathbf{F}^{n+1/2}_{\phi;\,i,j-1/2,k}\right) \\ &- \frac{\Delta t}{\Delta z}\left(\mathbf{F}^{n+1/2}_{z;\,i,j,k+1/2} - \mathbf{F}^{n+1/2}_{z;\,i,j,k-1/2}\right) + \Delta t\,\mathbf{S}^{n+1/2}_{ijk}.\end{aligned}$$

The FVM is coordinate-dependent, since it relies on the coordinate expansion of differential operators.

The only remaining geometric source term is $M_{\phi\phi}/R$ in the radial momentum equation, which includes the centrifugal force and magnetic tension terms.

FVM Update of the Geometric Source Term

$$\left\langle \frac{M_{\phi\phi}}{R} \right\rangle_{ijk}^{n+1/2} = \frac{1}{\Delta t\,\Delta V_{ijk}} \int_{t^n}^{t^{n+1}} \int_{V_{ijk}} \frac{\rho v_\phi^2 - B_\phi^2 + P^*}{R}\, dV\, dt. \tag{13}$$

Note that $P^* = P + B^2/2$ is the *total* pressure, $P = (\gamma-1)\epsilon$ is the gas pressure, and $\epsilon = E - \rho v^2/2 - B^2/2$ is the internal energy.

Computing source terms

For the P^* contribution, full FVM and CT updates are too costly. Instead, we compute

$$\left\langle \frac{P^*}{R} \right\rangle_{ijk} \approx \frac{R_{i+1/2}P^*_{i+1/2} + R_{i-1/2}P^*_{i-1/2}}{2R_i^2}.$$

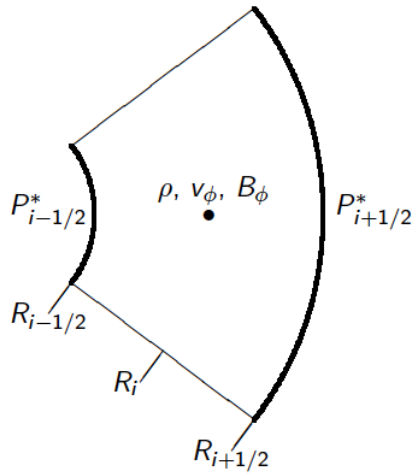

Test: rotational stability

We investigate the stability of rotating disks using a power-law rotation profile, $v_\phi(R) = \Omega_0 R^{1-q}$, where q is the shear parameter.

Rayleigh's criterion for rotational stability

$$\partial_R \left[(R^2\,\Omega(R))^2\right] > 0$$
$$\Rightarrow \quad q < 2$$

That is, angular momentum must increase with radius for stability with respect to angular velocity perturbations.

Test: rotational stability

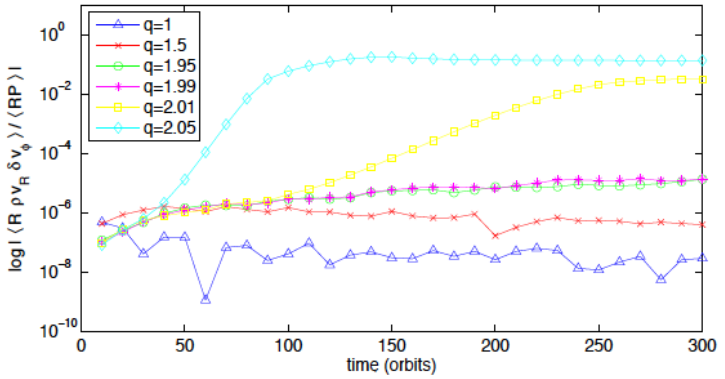

Figure: Mean dimensionless angular momentum transport as a function of time in the Rayleigh rotational stability test for various values of q.

Test: rotating wind solution

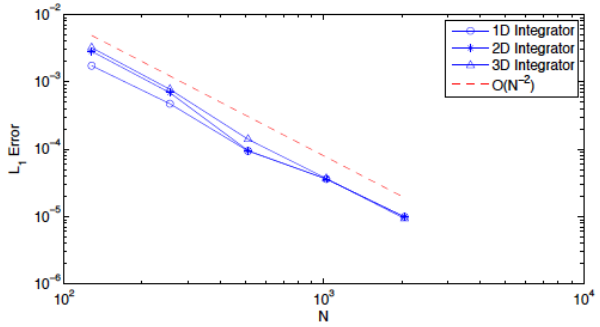

Figure: Convergence of the RMS error in the L_1-norm for various levels of discretization in 1D, 2D and 3D. The domain includes the slow- and fast-magnetosonic and Alfvén transitions.

Test: Field Loop advection

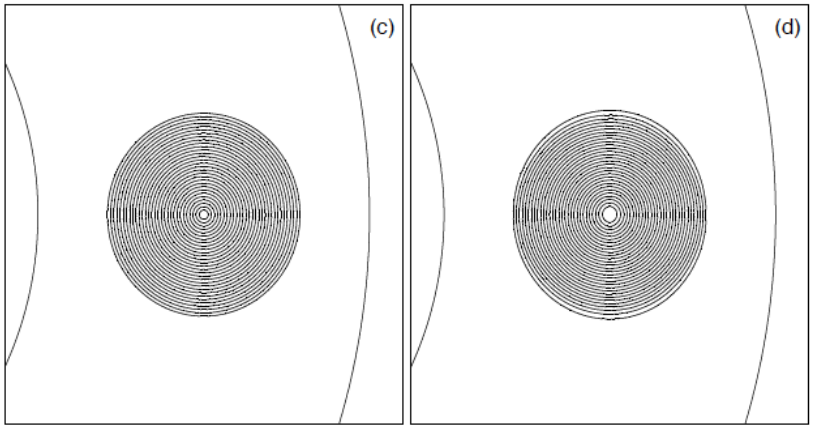

Figure: Magnetic field lines at $t = 0$ and $t = 2$.

Test: blast wave in strong field

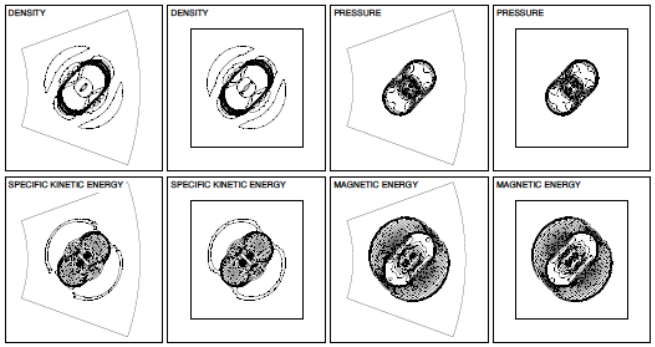

Figure: Contours of selected variables at time $t = 0.02$ for the 3D MHD blast wave test with $B_0 = 10$ and $\beta_p = 0.02$ using 200^3 grid cells and the cylindrical or Cartesian versions of *Athena*. Thirty equally spaced contours between the minimum and maximum are drawn in each plot.

Application: global MHD disk simulation of MRI

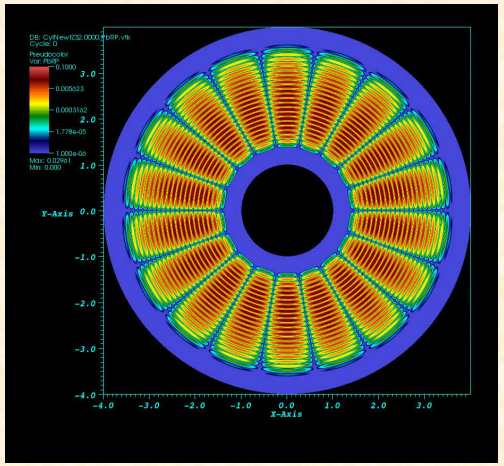

Sorathia et al 2012

Resolution in R,Φ,Z is 480x1920x128 (32 zones per scale height), evolution for 200 orbits at inner edge.

Static Mesh Refinement

Motivation: Static nested-grids are ideal to refine midplane in MHD studies of thin disks.

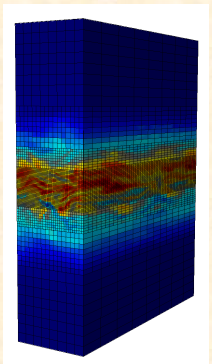

Density

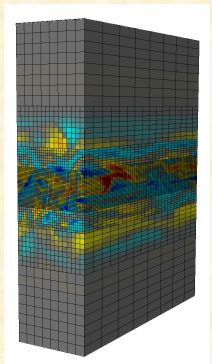

Angular momentum fluctuations

Prolongation

- At internal fine/coarse mesh boundary, boundary conditions for fine mesh must be interpolated from coarse grid: *prolongation*
- Requires multidimensional, conservative interpolation step.
- To keep div(B)=0, we use method of Toth & Roe (2002)

Restriction

- In regions of overlap, the coarse grid solution must be replaced by the fine grid solution (averaged to the coarse grid): *restriction*
- Requires simple conservative average.
- Restriction dramatically reduces amount of data to be passed between levels with MPI.
- Note: this means pressure (and temperature) is not the same between levels. Can have a big effect on microphysics. Danger, Will Robinson. Danger!

Flux-correction

- At fine/coarse mesh boundaries, coarse grid fluxes may not be equal to sum of fine grid fluxes.
- This can break conservation across mesh hierarchy
- Must update coarse grid cell at boundary using fine grid fluxes: *flux-correction*
- Must perform the CT update to correct field at fine/coarse boundaries while keeping div(B)=0. Implementation of correction with CT can be complex.

Tests of SMR

Tested with the complete Athena MHD test suite.

Example: Linear wave convergence with fixed refinement region.

- Initialize pure eigenmode for each wave family
- Measure RMS error in U after propagating one wavelength
- *quantitative* test of accuracy of scheme

Grid has fixed fine-level region

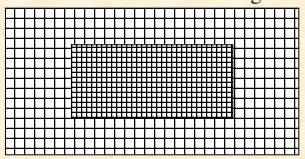

V_y in fast magnetosonic wave

No reflections at fine/coarse boundaries!

Linear wave convergence: fixed grid and SMR.

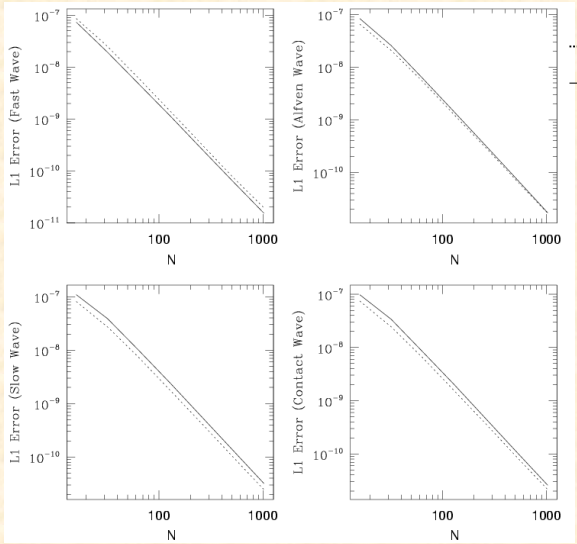

No increase in errors with SMR!

Implementation

Details are given at:

https://trac.princeton.edu/Athena/wiki/AthenaDocsUG

Summary

- Grid codes generate solutions which are Galilean invariant
- Substantial changes are required for cylindrical coordinates
- Static mesh refinement for CT MHD has been implemented but not for all physics options
- Future:
  - Generalized curvilinear coordinates (GR)
  - Adaptive mesh refinement (AMR)